

Computational Study of the Interactions between Guanine Derivatives and Cyclin-Dependent Kinase 2 (CDK2) by CoMFA and QM/MM

Jans Alzate-Morales and Julio Caballero*

Centro de Bioinformática y Simulación Molecular, Universidad de Talca, 2 Norte 685, Casilla 721, Talca, Chile

Received August 11, 2009

Comparative molecular field analysis (CoMFA) and QM/MM hybrid calculations were performed on 9*H*-purine derivatives as CDK2 inhibitors. CoMFA was carried out to describe the activities of 78 analogues. The models were applied to a training set including 64 compounds. The best CoMFA model included steric and electrostatic fields, had a good Q^2 value of 0.845, and adequately predicted the compounds contained in the test set. Furthermore, plots of the steric CoMFA field allowed conclusions to be drawn for the choice of suitable inhibitors. In addition, the dynamical behavior of compounds with 4-(aminosulfonyl)phenyl, 4-[(methylamino)sulfonyl]phenyl, 4-[(dimethylamino)sulfonyl]phenyl, and [3-methoxy-4-(aminosulfonyl)]phenyl groups at position 2 of the 9*H*-purine scaffold inside the CDK2 active site were analyzed by QM/MM calculations. The interactions of these compounds with residues Lys89, Asp86, and Ile10 were characterized.

INTRODUCTION

Cyclin-dependent kinases (CDKs), a family of serine–threonine protein kinases, are recognized as key regulatory elements in cell cycle progression (CCP).¹ They are sequentially activated through their association with regulatory subunits named cyclins and phosphorylation on specific amino acids on the activation loop (T-loop). CCP consists of two main phases: the interphase and mitosis (M). The CDKs needed for the different phases are contained in the cell at a constant level; however, the levels of cyclins fluctuate during CCP.² The increase of specific cyclins allows the formation of different CDK–cyclin complexes, which are activated and phosphorylate specific substrates. In this way, cyclins act as regulators at precise moments of the CCP.³ Abnormal CDK control of the cell cycle, resulting in aberrant cellular proliferation, has been strongly linked to the molecular pathology of cancer; for this reason, pharmacological inhibition of CDKs might provide an effective method for controlling tumor growth and, hence, an effective weapon in cancer chemotherapy.⁴

Most of the already-known CDK inhibitors (CDKIs) are small heterocycles that act by competing with adenosine triphosphate (ATP) for the kinase catalytic site. The design of inhibitors specific to a particular protein kinase was originally thought of as an impossible task owing to the high degree of homology shared by the ATP-binding domains of these enzymes. Actually, several CDKIs have entered clinical evaluation for the treatment of cancer.⁵ These include flavopiridol,⁶ 7-hydroxystaurosporine (UCN-01),⁷ roscovitine (CYC202),⁸ and an aminothiazole compound (BMS-387032).⁹ The identified CDKIs induce apoptosis and display antimitotic properties and are being evaluated as potential antitumor agents.^{5,10} Several preclinical studies have demonstrated that CDKIs, when used in combination with cytotoxic drugs, can re-establish an otherwise deficient cell

cycle checkpoint, which might enhance the activity of conventional treatments.¹¹ With these precedents, novel CDKIs with improved activity and selectivity are desired.

The increase in the speed and efficiency of drug discovery has seen huge investments by major pharmaceutical companies, with the primary aim of reducing cost per synthesized compound or assay. Drug discovery research is guided by high-throughput systems, automated assays, robotics, and advanced computational chemistry. Computational applications are essential for rational drug design. Models that are able to explain the interactions and predict the biological activity of compounds by their structural properties are powerful tools for designing highly active molecules.

Recently, one of the present authors (Caballero) and his co-workers reported quantitative structure–activity relationship (QSAR) models for predicting the inhibitory activities of CDK inhibitors.^{12–14} These models were achieved by using nonlinear difficult-to-interpret methods such as artificial neural networks^{12–14} and linear highly interpretable methods such as CoMFA¹⁵ (comparative molecular field analysis) and CoMSIA¹⁶ (comparative molecular similarity indices analysis). The predictive capabilities of these models were demonstrated according to statistical tests. In these reports, the authors made a comprehensive review of the state of the art concerning CDK inhibition QSAR modeling. In another report, the other present author (Alzate-Morales) and his co-workers determined the protein–ligand interaction energy between CDK2 and five 6-(cyclohexylmethoxy)-9*H*-purine derivatives by using the quantum mechanics/molecular mechanics (QM/MM) method.¹⁷ They obtained a correlation between the QM/MM interaction energy and the biological activity for these compounds. The same authors used reactivity indices defined in terms of the density of states for describing the affinity of the above-mentioned inhibitors for the CDK2 active site.¹⁸ Quite recently, Alzate-Morales et al. combined DOCKING and ONIOM (“our own N-layered integrated molecular orbital and molecular mechanics”) methodologies for establishing a structure–activity

* Corresponding author phone: 56-71-201 685; fax: 56-71 201 662; e-mail: jcaballero@utalca.cl or jmcr77@yahoo.com.

relationship for a set of 80 9*H*-purine derivatives.¹⁹ They predicted the orientations of different ligands within the CDK2 binding site by docking protocols, and then, they used the best ligand poses to perform hybrid quantum calculations within the ONIOM approach. They found that the main energy contribution to the total interaction energy between the protein and the ligand in the ONIOM model was given by the hydrogen-bond interactions between the ligands and residues at the entrance of the binding site (especially Lys89 and Asp86). In the current work, we studied the structure–activity relationships for 78 of the above-mentioned 9*H*-purine derivatives by using CoMFA analysis. Additionally, we analyzed the dynamical behavior of the hydrogen-bond (HB) interactions for some selected compounds (**29**, **42**, **43**, and **46**) with residues Lys89, Asp86, and Ile10 by using QM/MM. Previously, we identified that the 4-(aminosulfonyl)phenyl group at position 2 of the 9*H*-purine scaffold of compound **29** interacts with these residues. A small modification on the 4-(aminosulfonyl)phenyl group, as in compounds **42**, **43**, and **46**, deteriorates the activity. By means of a comparison of the selected systems, we gained further insight into the role played by the 4-(aminosulfonyl)phenyl group in the ligand affinity for the CDK2 binding site.

METHODOLOGY AND COMPUTATIONAL DETAILS

CoMFA Analysis. Compound structures and inhibitory activities on the T160pCDK2–cyclinA enzymatic system of 80 6-(cyclohexylmethoxy)-9*H*-purine derivatives used in this study are reported in Table 1, and they were extracted from articles by the same research group.^{20–23} For modeling, IC₅₀ activities were converted into logarithmic activities, log(10³/IC₅₀). Three-dimensional conformations previously obtained from docking simulations achieved in ref 19 were used for CoMFA analysis. This guaranteed that all compounds were aligned in the CDK2 active site.

QSAR modeling was performed using the Sybyl 7.3 software of Tripos.²⁴ The data set was divided into two data subsets (64 and 14 compounds were in the training and test sets, respectively) for external validation process. The molecules of the training set were placed in a rectangular grid extended beyond 4 Å in each direction from the coordinates of each molecule. The interaction energies between a probe atom (an sp³-hybridized carbon atom with +1 charge) and all compounds were computed at the surrounding points, using a volume-dependent lattice with 2.0-Å grid spacing. Then, standard Sybyl parameters were used for a partial least-squares (PLS) analysis. The number of components in the PLS models was optimized using the *Q*² value, obtained from the leave-one-out (LOO) cross-validation procedure, with the SAMPLS²⁵ sampling method. The number of components was increased until additional components did not increase *Q*² by at least 5% per added component. The CoMFA models were generated by using steric and electrostatic probes with standard 30 kcal/mol cutoffs.

QM/MM Simulations. Molecular dynamics of compounds **29** (NU6102), **42**, **43**, and **46** inside the CDK2 active site were studied by QM/MM simulations. All simulations were performed using the DYNAMO software package.²⁶ The initial coordinates for the QM/MM calculations were taken from the docking experiments. To mimic the aqueous

environment, an equilibrated water box with sides of 79.5 Å, centered on the mass center of each inhibitor, was used to solvate the T160pCDK2–cyclinA–ligand system. Amino acid residues and water molecules placed more than 25 Å away from the center of the box were fixed during the simulations. The inhibitors inside the ATP active site were chosen to be the QM subsystem, described at the AM1 level,²⁷ whereas the rest of the T160pCDK2–cyclinA complex and the water molecules of crystallization and those belonging to the solvent box constitute the MM subsystem and were described using the optimized potential for liquid simulations (OPLS) force field²⁸ and the flexible TIP3P potential,^{29,30} respectively.

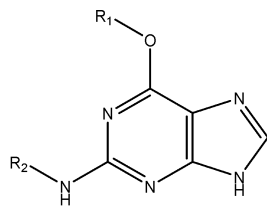
There are no bonds between the QM and the MM subsystems, so we do not need to consider any special treatment to complete the valence of the frontier quantum atoms.³¹ Initially, the hydrogen atoms of the system were relaxed using the conjugate gradient subroutine implemented in the DYNAMO program. Then, the full system was minimized up to a gradient tolerance of 1.0 kJ/mol. Subsequently, the system was heated to 300 K by a sequence of molecular dynamics (MD) simulations. Afterward, the system was further equilibrated during an additional 100 ps using the NVT ensemble at 300 K. The production run consisted of an MD simulation of 500 ps. In all cases, we used a time step of 1 fs to solve the equations of motion and a switched cutoff distance of 13.5 Å. One protein–ligand configuration was saved each 15 time steps for a posteriori energetic and structural analysis. The interaction energy and its components (electrostatic and van der Waals), for selected compounds against CDK2, were obtained according to the procedure described by us in a previous work.¹⁷

RESULTS AND DISCUSSION

CoMFA Modeling. CoMFA models were applied to obtain information about the structural features and properties affecting the CDK2 inhibitory activity of the guanine derivatives. The chosen conformations of the inhibitors play a crucial role in three-dimensional QSAR model building. Therefore, entire structures have to be properly aligned to produce a predictive model. The alignment was achieved previously by docking each inhibitor to a fixed conformation of CDK2 (as represented in Figure 3 of ref 19); this allowed the CoMFA coefficient contour maps to be superimposed on the active site of CDK2. First, we developed the CoMFA models by including one field, and then, we combined these fields and analyzed the statistical quality of hybrid models by considering *Q*² values.³² The results are presented in Table 2. The CoMFA model describing CDK2 inhibition that used only a steric field (model CoMFA-S) had a *Q*² value of 0.801 using four components. On the other hand, when only an electrostatic field was used (model CoMFA-E), the obtained model had a *Q*² value of 0.785 using 10 components. Finally, when both fields were considered (model CoMFA-SE), a CoMFA model with higher statistical significance (*Q*² = 0.845) was obtained. These results reveal that both steric and electrostatic features of the studied molecules have a major influence on the CDK2 inhibitory activity. The model indicated a steric contribution of 55.5% and an electrostatic contribution of 44.5%. The predictions of log(10³/IC₅₀) values for the 64 guanine derivatives using model CoMFA-SE are

Table 1. Experimental and Predicted CDK2 Inhibitory Activities [$\log(10^3/\text{IC}_{50})$ (μM)] of Guanine Derivatives Using CoMFA Model^a

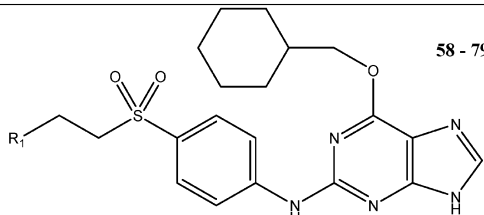
1 - 57



Compound ^a	R ₁	R ₂	Log(10 ³ /IC ₅₀)		
			Exp	Predicted	LOO-predicted
1	n-C ₃ H ₇	H	1.174	1.204	1.406
2	n-C ₄ H ₉	H	1.319	1.387	1.440
3	n-C ₅ H ₁₁	H	1.310	1.376	1.403
4	i-C ₃ H ₇	H	1.125	1.298	1.501
5	sec-C ₄ H ₉	H	1.602	1.442	1.271
6	i-C ₄ H ₉	H	1.377	1.385	1.428
7	C ₂ H ₅ CH(CH ₃)CH ₂	H	1.824	1.791	1.709
8	i-C ₅ H ₁₁	H	1.585	1.508	1.430
9	2-propynyl	H	ND	ND	ND
10^a	5-hexenyl	H	1.328	1.724	-
11	t-3-hexenyl	H	1.161	1.219	1.304
12	allyl	H	ND	ND	ND
13	2-CH ₃ -2-propenyl	H	1.456	1.443	1.444
14	2-C ₂ H ₅ -2-propenyl	H	1.678	1.594	1.530
15	2-i-C ₃ H ₇ -2-propenyl	H	1.796	1.761	1.678
16	2-Ph-2-propenyl	H	1.469	1.469	1.646
17^a	cyclopentylmethyl	H	1.678	1.477	-
18	1-cyclopenten-1-ylmethyl	H	1.509	1.595	1.744
19	1-cyclohexen-1-ylmethyl	H	1.658	1.756	1.973
20^a	3-cyclohexen-1-ylmethyl	H	1.796	1.740	-
21	2-cyclohexylethyl	H	1.357	1.348	1.377
22^a	Bn	H	1.456	1.511	-
23^a	2-phenylethyl	H	1.187	1.483	-
24	2,2-diethoxypropyl	H	1.481	1.433	1.404
25	2,2-dimethoxybutyl	H	1.699	1.665	1.600
26	(2-i-C ₃ H ₇ -1,3-dioxolan-2-yl)methyl	H	1.187	1.208	1.569
27	cyclohexylmethyl	H	1.770	1.746	1.608
28	cyclohexylmethyl	Ph	3.013	2.745	2.312
29	cyclohexylmethyl	4-(aminosulfonyl)phenyl	5.268	5.260	4.801
30	cyclohexylmethyl	CH ₃	2.301	2.117	1.788
31	cyclohexylmethyl	C ₂ H ₅	2.553	2.713	2.771
32	cyclohexylmethyl	i-C ₃ H ₇	2.921	2.931	2.741
33	cyclohexylmethyl	2-hydroxyethyl	2.553	2.581	2.574
34	cyclohexylmethyl	3-chlorophenyl	2.638	2.626	2.782
35	cyclohexylmethyl	3-bromophenyl	2.167	2.303	2.912
36	cyclohexylmethyl	3,5-dichlorophenyl	1.921	2.051	3.112
37	cyclohexylmethyl	3-(hydroxymethyl)phenyl	3.398	3.472	2.742
38	cyclohexylmethyl	3-methoxyphenyl	2.745	2.683	2.693
39	cyclohexylmethyl	3-(methylsulfanyl)phenyl	2.770	2.729	2.614
40^a	cyclohexylmethyl	4-hydroxyphenyl	4.161	3.389	-
41	cyclohexylmethyl	4-methoxyphenyl	3.187	3.185	3.367

Table 1. Continued

Comp ound ^a	R ₁	R ₂	Log(10 ³ /IC ₅₀)		
			Exp	Predicted	LOO- predicted
42	cyclohexylmethyl	4-[(methylamino)sulfonyl]phenyl	5.155	5.190	4.809
43	cyclohexylmethyl	4-[(dimethylamino)sulfonyl]phenyl	4.252	4.130	3.498
44	cyclohexylmethyl	4-(methylsulfonyl)phenyl	4.201	4.327	4.469
45	cyclohexylmethyl	4-(methysulfinyl)phenyl	4.000	4.012	3.264
46	cyclohexylmethyl	[3-methoxy-4-(aminosulfonyl)]phenyl	4.155	4.103	3.692
47	cyclohexylmethyl	3-(aminosulfonyl)phenyl	3.678	3.700	2.611
48	cyclohexylmethyl	4-(aminocarbonyl)phenyl	4.194	4.092	3.611
49	cyclohexylmethyl	4-[(methylamino)carbonyl]phenyl	3.699	3.933	4.191
50	cyclohexylmethyl	4-[(dimethylamino)carbonyl]phenyl	3.699	3.669	3.652
51^a	cyclohexylmethyl	4-acetylphenyl	3.523	3.905	-
52	cyclohexylmethyl	4-carboxyphenyl	3.097	3.012	3.6
53^a	cyclohexylmethyl	4-(2-amino-2-oxoethyl)phenyl	3.886	3.536	-
54	cyclohexylmethyl	4-(cyanomethyl)phenyl	3.523	3.511	3.466
55^a	cyclohexylmethyl	2-thienylmethyl	2.770	3.060	-
56^a	cyclohexylmethyl	[5-(aminosulfonyl)-2-thienyl]methyl	2.301	3.343	-
57	cyclohexylmethyl	4-(aminosulfonyl)anilino	2.367	2.469	2.908



Comp ound	R ₁	Log(10 ³ /IC ₅₀)		
		Exp	Predicted	LOO- predicted
58	4-morpholinyl	3.796	3.825	3.761
59	4-methyl-1-piperazinyl	3.921	3.902	3.254
60	1-piperidinyl	3.469	3.503	3.534
61	4-thiomorpholinyl	3.268	3.152	3.56
62^a	Diethylamino	3.347	3.661	-
63	(2 <i>R</i> ,6 <i>S</i>)-2,6-dimethylmorpholinyl	3.347	3.322	4.173
64	(3-hydroxypropyl)amino	4.347	4.404	3.734
65^a	(2-hydroxyethyl)amino	4.328	3.836	-
66	Cyclopentylamino	4.638	4.627	4.243
67	(dibutylamino)ethyl	2.432	2.374	3.286
68	[2-(acetylamino)ethyl]amino	4.108	4.099	3.38
69^a	4-i-C ₃ H ₇ -1-piperazinyl	3.469	3.701	-
70	4-(2-hydroxyethyl)-1-piperazinyl	3.585	3.559	3.376
71	4-(2-hydroxyethyl)-1-piperidinyl	3.620	3.670	2.936
72	4-[2-(2-hydroxyethoxy)ethyl]-1-piperazinyl	3.509	3.460	3.605
73^a	4-ethyl-1-piperazinyl	3.585	3.315	-
74	4-acetyl-1-piperazinyl	3.638	3.655	3.731
75	[2-(dimethylamino)ethyl](methyl)amino	3.602	3.519	3.995
76	1-azepanyl	2.750	2.775	3.381
77	4-(2-methoxyethyl)-1-piperazinyl	3.538	3.594	3.446
78	1-pyrrolidinyl	3.745	3.693	3.617
79	bis(2-hydroxyethyl)amino	3.959	3.987	3.701

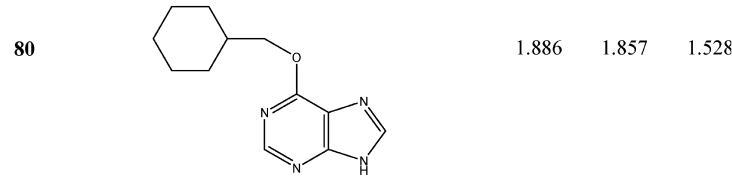
^a Denotes test-set compounds.

Table 2. CoMFA Analysis Results^a

	NC	R^2	S	F	Q^2	S_{cv}	fraction	
							steric	electrostatic
CoMFA-S	4	0.943	0.278	243.53	0.801	0.519	1	
CoMFA-E	10	0.990	0.120	545.22	0.785	0.569		1
CoMFA-SE	7	0.994	0.089	1416.92	0.845	0.471	0.555	0.445

^a NC is the number of components from the PLS analysis; R^2 is the square of the correlation coefficient; S is the standard deviation of the regression; F is the Fischer ratio; and Q^2 and S_{cv} are the correlation coefficient and standard deviation, respectively, of the leave-one-out (LOO) cross-validation.

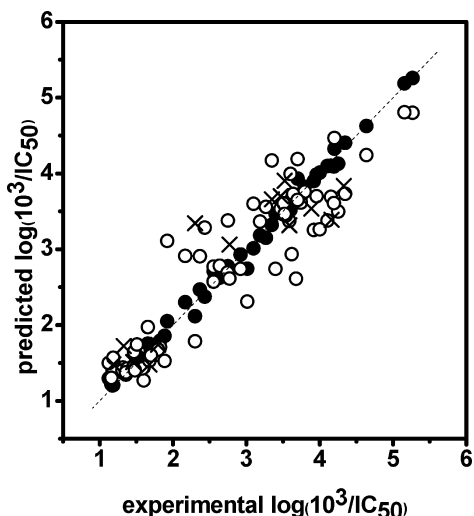


Figure 1. Scatter plot of the experimental activities versus predicted activities for model CoMFA-SE: (●) training-set predictions, (○) LOO cross-validated predictions, (×) test-set predictions.

reported in Table 1. The correlations between the calculated and experimental values of $\log(10^3/\text{IC}_{50})$ (from training and LOO cross-validation) are shown in Figure 1. Model CoMFA-SE was also used to predict the inhibitory activities of the test-set compounds. We found that this model was able to describe the test-set variance with $R^2 = 0.833$. The test-set predicted values are listed in Table 1, and the correlations between the predictions and experimental values are represented in Figure 1. This analysis reveals that the proposed model is able to predict successfully compounds that were not used in the training process.

The contour plots of the CoMFA steric and electrostatic fields are presented in Figure 2. Although the contour plots should not be overinterpreted as receptor maps,¹⁵ a comparison of the contour plots and the CDK2 active site can help in delineating the properties of active compounds inside the active site of CDK2. In this sense, the superposition of CoMFA contour plots on active-site residues is shown in Figure 2. To aid in visualization, compound 29 is displayed in the maps. In general, the colored isopleths in the map surround all lattice points where the QSAR strongly associated changes in the compounds' field values with changes in biological potency.

Green and yellow isopleths indicate regions where bulky groups favored and disfavored the activity, respectively (Figure 2B). Large regions of green contour near the 4-(aminosulfonyl)phenyl moiety of compound 29 suggest that there is a favorable steric region between residues Ile10, Gln85, and Lys89. In fact, compounds with large substituents at position 2 of the 9*H*-purine scaffold are better inhibitors than compounds with an NH₂ substituent at this position. In

addition, some yellow isopleths surround the green isopleths mentioned above near the residues Gln131, Asp86, Leu87, and Gln85. This suggests that substituents that are too large are not desired in this zone. In fact, the presence of the 4-(aminosulfonyl)phenyl moiety or similar substituents seems to be adequate for having a good inhibitor [compounds 29 and 42 have $\log(10^3/\text{IC}_{50})$ values above 5]; however, compounds with bulkier substituents are less active [for instance, compounds 58, 61, and 70, among others, have $\log(10^3/\text{IC}_{50})$ values below 4]. Other yellow contours near the cyclohexylmethoxy moiety at position 6 of 9*H*-purine scaffold suggest that there are unfavorable steric regions near residues Leu134 and Asn132; the backbone of Gly11 and Ile10; and the pocket located between residues Lys33, Ala144, Phe80, and Val64. The cyclohexylmethoxy moiety has adequate dimensions for occupying this position; however, other substituents, such as *n*-butoxy (compound 2), *n*-pentoxy (compound 3), 2-methylbutoxy (compound 7), 2-cyclohexylethoxy (compound 21), are not beneficial to the inhibitory activity. It is obvious that the binding site near the above-mentioned residues is quite sterically restricted.

Blue and red isopleths indicate regions where positive and negative charges, respectively, favored the activity (Figure 2C). Blue contours are observed in the surroundings of 4-(aminosulfonyl)phenyl moiety of compound 29. Some of them are near backbone of residues Asp86 and Gln85, and the other is near residue Ile10. These isopleths indicate that positively charged groups such as NH₂ of the 4-(aminosulfonyl)phenyl moiety in compound 29 favor the activity. Other active compounds such as 42 [$\log(10^3/\text{IC}_{50}) = 5.155$] and 46 [$\log(10^3/\text{IC}_{50}) = 4.155$] contain NH₂ or NHCH₃ groups in this zone. Another blue isopleth is located near residues Ala144 and Asp145, which suggests that positively charged groups on the cyclohexylmethoxy moiety at position 6 of the 9*H*-purine scaffold should increase the activity. On the other hand, two red contours were observed near the sulfonyl group in the 4-(aminosulfonyl)phenyl moiety of compound 29 and Lys89. The zone containing these isopleths is occupied by sulfonyl oxygen atoms in the most active compounds.

Interactions of Aminosulfonyl Group with Residues Lys89, Asp86 and Ile10 by QM/MM Calculations. The most active compound in our data set (compound 29) contains a 4-(aminosulfonyl)phenyl group at position 2 of the 9*H*-purine scaffold, which seems to be an ideal group for establishing HB interactions with residues Lys89, Asp86, and Ile10. According to the CoMFA results, both steric and electrostatic features are located in the pocket near these residues, but CoMFA is not an adequate method for explaining why the 4-(aminosulfonyl)phenyl group has better interactions in this pocket than other similar groups. Com-

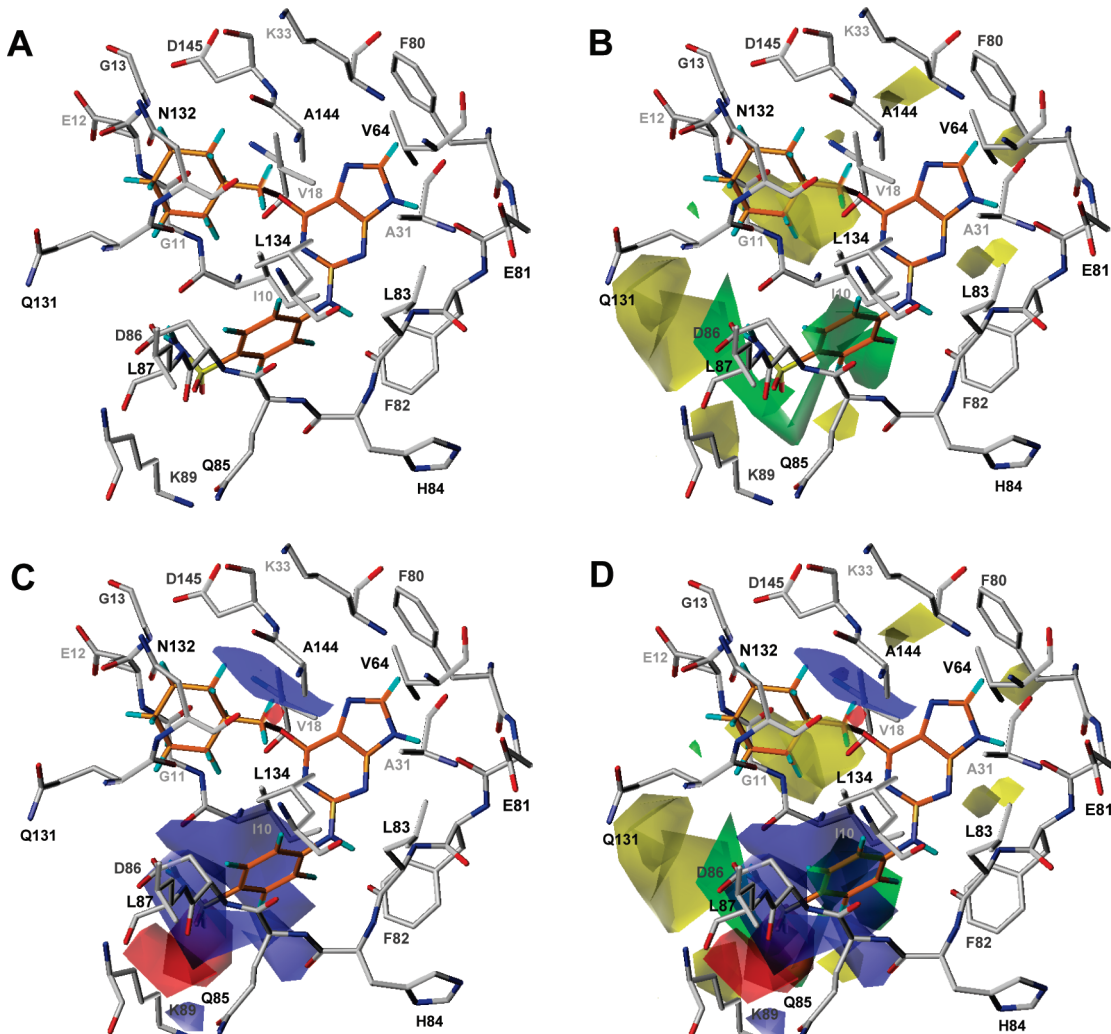


Figure 2. Comparison between the PLS coefficient maps and the amino acid residues located close to the binding pocket of CDK2. Compound **29** is shown inside the field. (A) Complex between compound **29** and CDK2 active site, (B) steric field, (C) electrostatic field, (D) both fields. Green isopleths indicate regions where bulky groups enhance the activity, and yellow isopleths indicate regions where bulky groups disfavor the activity. Blue isopleths indicate regions where an increase of positive charge enhances the activity, and red isopleths indicate regions where more negative charges are favorable for activity.

ounds **42**, **43**, and **46** are similar to compound **29**, but they have some modifications in the aminosulfonyl group that make them less active. In the second part of our work, the dynamics of the HB interactions between the aminosulfonyl group and residues Lys89, Asp86, and Ile10 of CDK2 were studied for compounds **29**, **42**, **43**, and **46** using QM/MM simulations. The aim is to obtain a more precise depiction of these interactions.

Compounds **29**, **42**, **43**, and **46** were selected from the data set because of the considerable differences in their activities against CDK2 (nanomolar range) and their small differences in the substitution and structural characteristics of the 4-(aminosulfonyl)phenyl group. The aqueous environment was also considered. Compound **29** (NU6102) is the most active in our data set [$\log(10^3/\text{IC}_{50}) = 5.268$] and contains the 4-(aminosulfonyl)phenyl moiety at this position. Compound **42** has a methyl group substituting one hydrogen of the aminosulfonyl group and shows slightly less activity [$\log(10^3/\text{IC}_{50}) = 5.155$]. Compound **43** has two methyl groups substituting the hydrogens of the aminosulfonyl group and shows still less activity than compounds **29** and **42** [$\log(10^3/\text{IC}_{50}) = 4.252$]. Finally, compound **46** has a methoxy substituent at position 3 of the phenyl group in the 4-(ami-

nosulfonyl)phenyl moiety and also has a lower activity than compound **29** [$\log(10^3/\text{IC}_{50}) = 4.155$]. The impact of these structural differences on the ligand affinity is important, and it is assumed to occur because of the differences in the HB interaction network with residues at the ATP solvent channel, as proposed previously according to available crystallographic data.²⁰ However, there exist some discrepancies about the roles of some of those residues in the affinity and selectivity of the ligands by CDK2. We aim to provide further insight into this topic in the present analysis.

The root-mean square deviations (rmsd's) of the positions for all backbone atoms from their initial configuration as a function of simulation time for all of the investigated systems are shown in Figure 3. The dependences of the rmsd values were tested to check whether convergence of the calculations was obtained and whether the MD trajectory was stable. The rmsd values remain within 0.45 Å for all systems; this demonstrates the conformational stabilities of the protein structures. During all simulations, the studied compounds were in the expected orientations. In all simulations, the purine ring was in the right position to establish the typical triplet of HB interactions with the backbone structure of residues Glu81 and Leu83. NH-9 acts as a hydrogen-bond

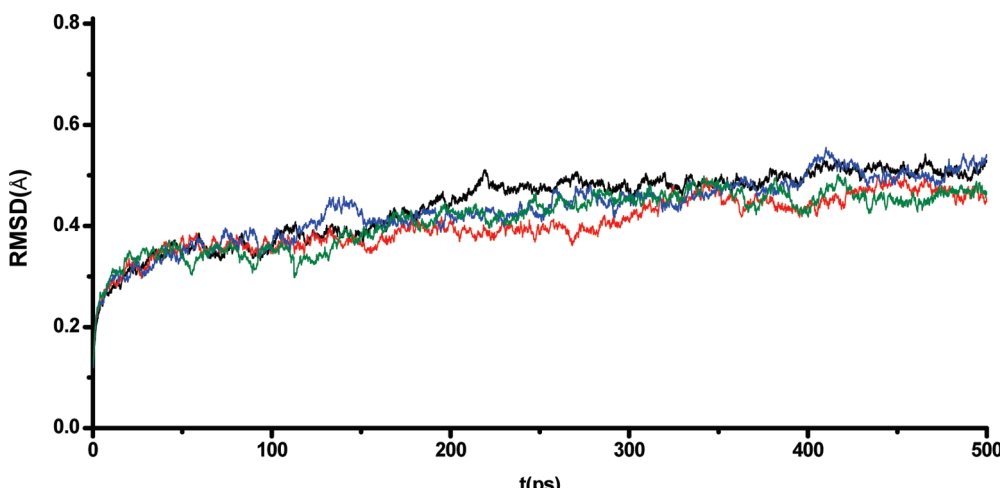


Figure 3. Time dependence of the root-mean-square deviations (rmsd's) for the backbone from starting structures. rmsd values for systems containing compounds **29**, **42**, **43**, and **46** are represented in black, red, blue and green, respectively.

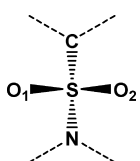


Figure 4. Identification of sulfonyl oxygens.

donor to the backbone carbonyl group of Glu81, and N3 and NH substituting position 2 of the 9*H*-purine scaffold accept and donate a hydrogen bond to the backbone carbonyl and amide groups, respectively, of Leu83.²³ We analyzed the hydrogen bonds formed between the groups at the 4-(aminosulfonyl)phenyl moiety of the inhibitors and some residues at the ATP solvent channel within the CDK2 binding site. For clarity, we denote the sulfonyl oxygens as O₁ and O₂ as represented in Figure 4.

In a recent article, Hardcastle et al. reported that compound **29** (NU6102) interacts with Asp86 through the NH₂ group of the aminosulfonyl group, which donates a HB to the side-chain oxygen of Asp86, and through one sulfonamide oxygen, which accepts a hydrogen bond from the backbone nitrogen of Asp86.²⁰ They further suggested that the high activity of this compound is due to the two additional HBs formed with Asp86. However, more recently, we found that the interactions formed for this compound inside the active site of CDK2 are different from those reported previously.¹⁷ We found that the NH₂ group of the sulfonamide donates a HB to each of the side-chain oxygen atoms of Asp86, one sulfonamide oxygen atom (O₁) accepts a HB from the NH₃⁺ side-chain group of Lys89, and the other sulfonamide oxygen atom (O₂) interacts with the backbone carbonyl group of residue Ile10 mediated by a water molecule from the solvent water box.

To trace the motion and dynamics for these interactions and to determine whether the HBs were formed or broken, the interatomic distances describing them were monitored during the four developed QM/MM simulations. Snapshots of the conformations obtained in each simulation are shown in Figure 5 for each complex. Figure 6A shows the distance between the sulfonamide oxygen O₁ and the nitrogen from the NH₃⁺ side-chain group of Lys89 [D(O₁S—NLys89)] for all of the complexes. It can be seen that this interatomic distance did not show significant changes until 500 ps for

compound **29**. D(O₁S—NLys89) takes values around 2.8 Å throughout the simulation, which suggests that the HB between the aminosulfonyl group of compound **29** and the side chain of Lys89 (Figure 5A) is quite stable. Interestingly, D(O₁S—NLys89) takes values around 5.7 Å for compounds **42** and **43** throughout their simulations, which suggests that the presence of methyl groups in the amino of the aminosulfonyl group obstructs the possibility of forming HBs with the side chain of Lys89 of CDK2 (Figure 5B,C). Finally, D(O₁S—NLys89) takes values around 2.8 Å for compound **46** until 390 ps, after which the interaction was broken. According to this result, compound **46** forms a HB between O₁ and the side chain of Lys89, but the presence of a bulky substituent on the phenyl ring in the 4-(aminosulfonyl)phenyl moiety has a negative influence on the stability of this interaction (Figure 5D,E).

Figure 6B shows the distance between the nitrogen from the aminosulfonyl group of the inhibitor and the carboxylic carbon from side-chain group of Asp86 [D(N—COAsp86)] for all of the studied complexes. We selected this distance for describing the HB between the nitrogen from the aminosulfonyl group and one of the carboxylic oxygens of Asp86 because the carboxylic oxygens of Asp86 are interchangeable; in this sense, a D(N—COAsp86) value between 3.5 and 4.5 Å means that the mentioned HB is formed. It can be seen that D(N—COAsp86) takes the mentioned values for compounds **29**, **42**, and **46** throughout their simulations, but takes higher values for compound **43**. These results suggest that the HB between the nitrogen from the aminosulfonyl group and one of the carboxylic oxygens of Asp86 is formed if the aminosulfonyl group has a HB donor group (Figure 5A,B,D,E). Because compound **43** does not fulfill this condition, it is not able to interact with Asp86 (Figure 5C). It is worth noting that the fact that the mentioned distance is not very stable for compound **46** might be due to the steric effects exerted by the methoxy group at position 3 of the phenyl ring.

Figure 6C shows the distance between the sulfonamide oxygen O₁ of the inhibitors and the nitrogen from the backbone of Asp86 [D(O₁S—NHAsp86)] for all of the studied complexes. It can be seen that this interatomic distance was between 4.5 and 6.5 Å for compound **29** throughout its 500-ps simulation. As was indicated previ-

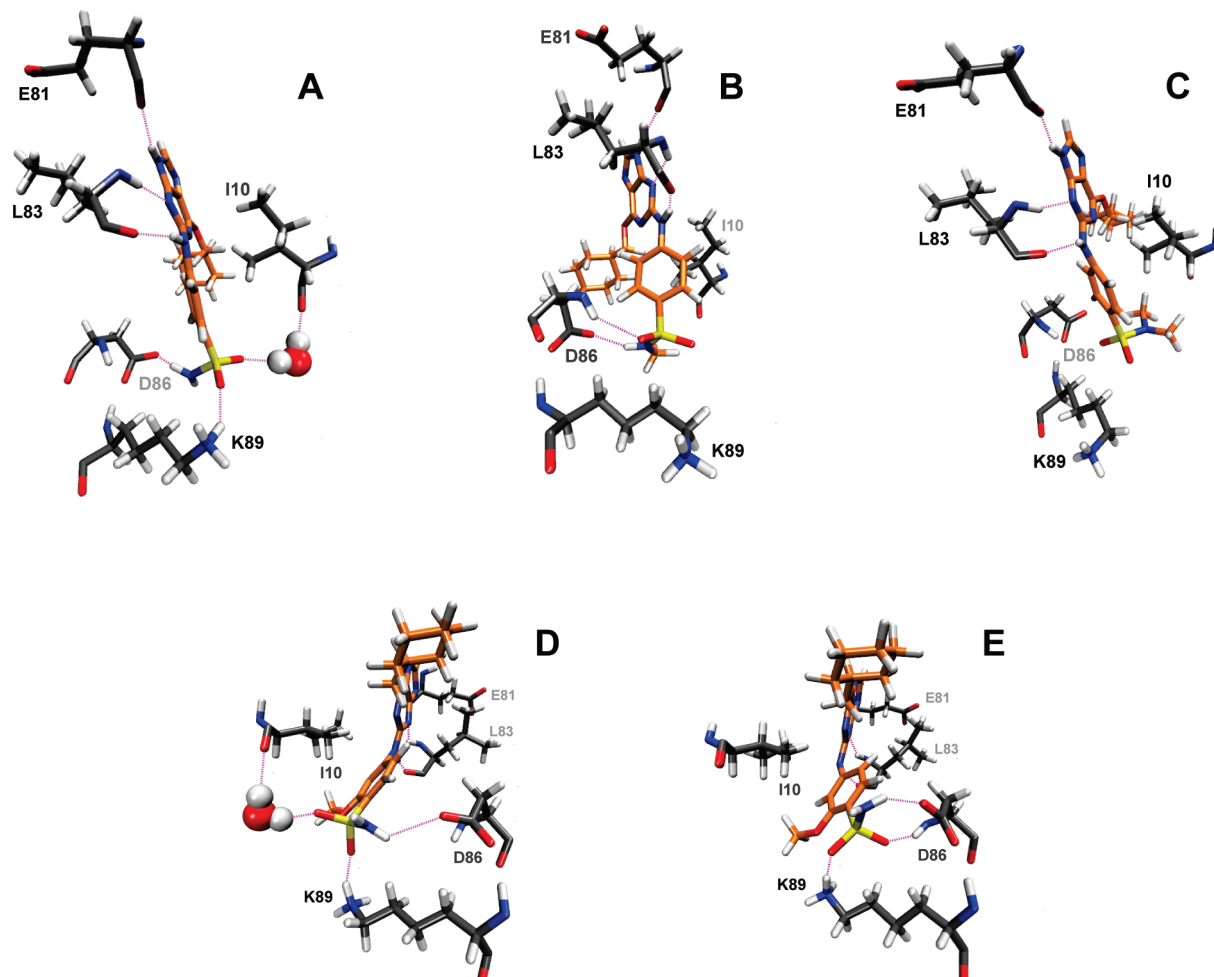


Figure 5. Hydrogen-bonding networks at the active site of the CDK2–inhibitor complex: (A) for compound **29**, (B) for compound **42**, (C) for compound **43**, (D) for compound **46** from 0 to 390 ps, and (E) for compound **46** from 390 to 500 ps.

ously, O₁ of compound **29** establishes a HB with the side chain of Lys89; for this reason, it cannot establish a HB with the backbone of Asp86 (Figure 5A). By contrast, $D(O_1S-NHAsp86)$ takes values around 3 Å for compound **42**, which definitely suggests that O₁ of this compound forms a HB with the nitrogen from the backbone of Asp86 (Figure 5B). On the other hand, $D(O_1S-NHAsp86)$ for compound **43** was around 3 and 5 Å throughout its simulation. Even though O₁ of compound **43** is near the nitrogen atom of Asp86 (Figure 5C), the plot in Figure 6C suggests that a HB between these atoms is formed only occasionally. In the complex between this compound and CDK2, methyl groups substituting the aminosulfonyl group of the ligand are accommodated inside a hydrophobic pocket near residue Ile10; this van der Waals interaction seems to be prioritized. Finally, $D(O_1S-NHAsp86)$ takes values around 4.5 and 6.5 Å for compound **46** until 390 ps; after that, it takes values around 3 Å. According to this result, before 390 ps, compound **46** behaves similarly to compound **29**: Its O₁ forms a HB with the side chain of Lys89 and does not form a HB with the backbone of Asp86 (Figure 5D). However, after 390 ps, it behaves similarly to compound **42**: Its O₁ forms a HB with the backbone of Asp86 (Figure 5E).

All of these partial results together suggest two important additional facts in regard to the hypothesis given by Hardcastle et al.²⁰ about the importance of the two hydrogen bonds formed by compound **29** with residue Asp86: First,

the HB interaction with the side chain of residue Asp86 seems to be determinant in achieving high affinity for CDK2, and second, the Asp86 backbone and the Lys89 side chain have a shared role as determinants in the affinity of compounds **29** and **42** for CDK2. It seems that the interaction with Lys89 gives slightly more stability to compound **29**, compared to compound **42**, within the CDK2 binding site. The behavior of compound **43** supports the findings of Hardcastle et al. that a single sulfonamide N–H is sufficient for optimal binding of the inhibitors to the enzyme.

During the 500-ps simulation for the complex between compound **46** and CDK2, this compound had the two orientations represented in Figure 5D,E. The first orientation had the above-mentioned HB interactions characterized by $D(O_1S-NLys89) \approx 2.8$ Å, $D(N-COAsp86) \approx 4$ Å, and a water-bridge HB interaction with Ile10 that we will discuss later. After 390 ps, the dihedral angle between the benzene ring and the SN bond in the aminosulfonyl group rotated, and new interactions were established that were characterized by $D(N-COAsp86) \approx 4$ Å, $D(O_1S-NHAsp86) \approx 3$ Å, and a HB interaction between the sulfonamide oxygen O₂ of the inhibitor and the nitrogen from NH₃⁺ side-chain group of Lys89, denoted as $D(O_2S-NLys89)$ (Figure 6D). $D(O_2S-NLys89)$ was around 2.8 Å after the reorientation of compound **46**.

The other sulfonamide oxygen atom O₂ showed different interactions with the residues of CDK2 for the selected

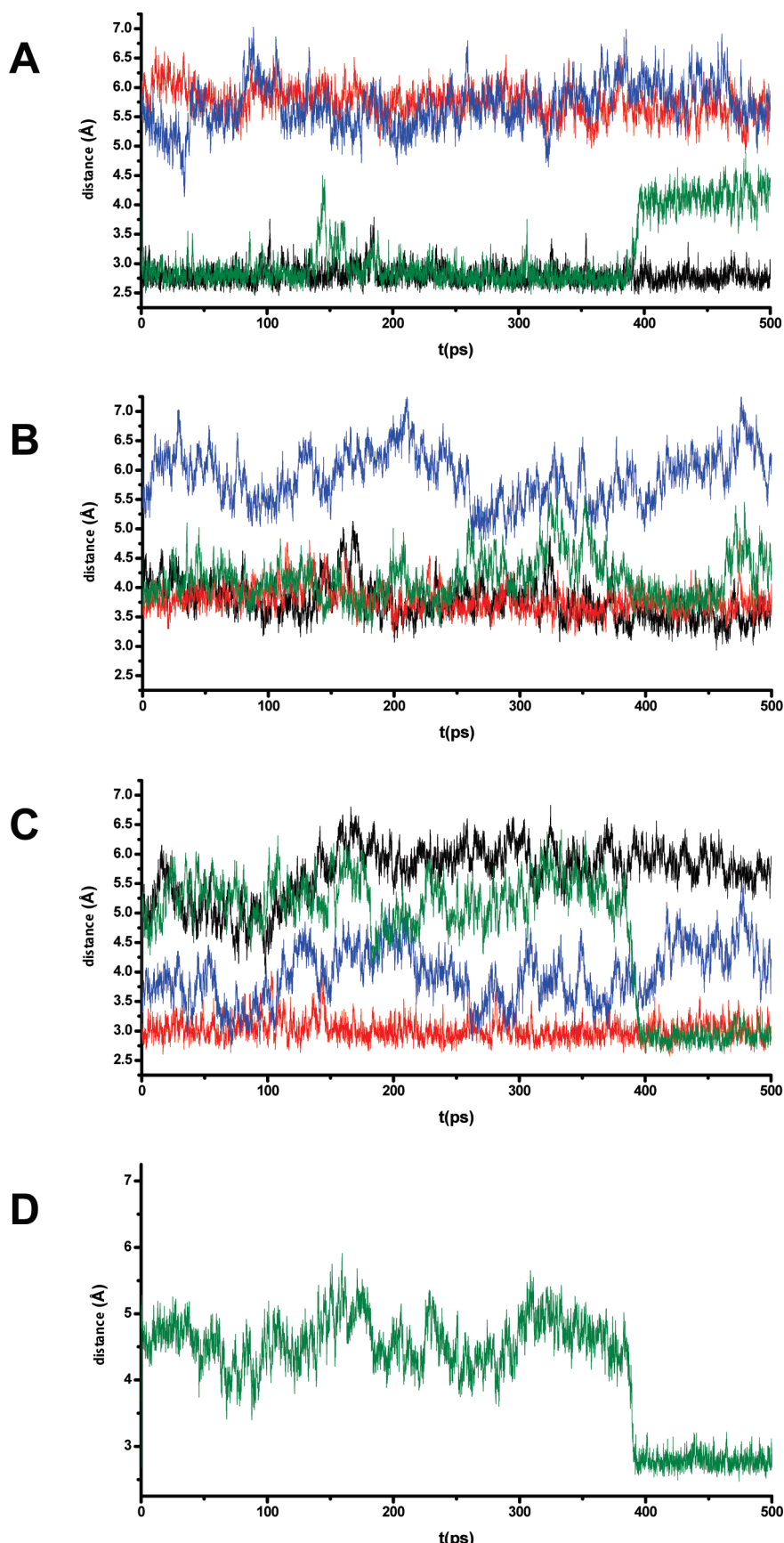


Figure 6. Distances between groups of inhibitor and residues of CDK2 for the complexes extracted from 500-ps QM/MM simulations. (A) Distances between the sulfonamide oxygen O₁ of the inhibitors and the nitrogen from the NH₃⁺ side-chain group of Lys89 [D(O₁S—NLys89)]. (B) Distances between the nitrogen from the aminosulfonyl group of the inhibitors and the carboxylic carbon from side-chain group of Asp86 [D(N—CO₂Asp86)]. (C) Distances between the sulfonamide oxygen O₁ of the inhibitors and the nitrogen from backbone of Asp86 [D(O₁S—NHA_{sp}86)]. (D) Distance between the sulfonamide oxygen O₂ and the nitrogen from NH₃⁺ side-chain group of Lys89 [D(O₂S—NLys89)] for compound **46**. Trajectories for compounds **29**, **42**, **43**, and **46** are represented in black, red, blue, and green, respectively.

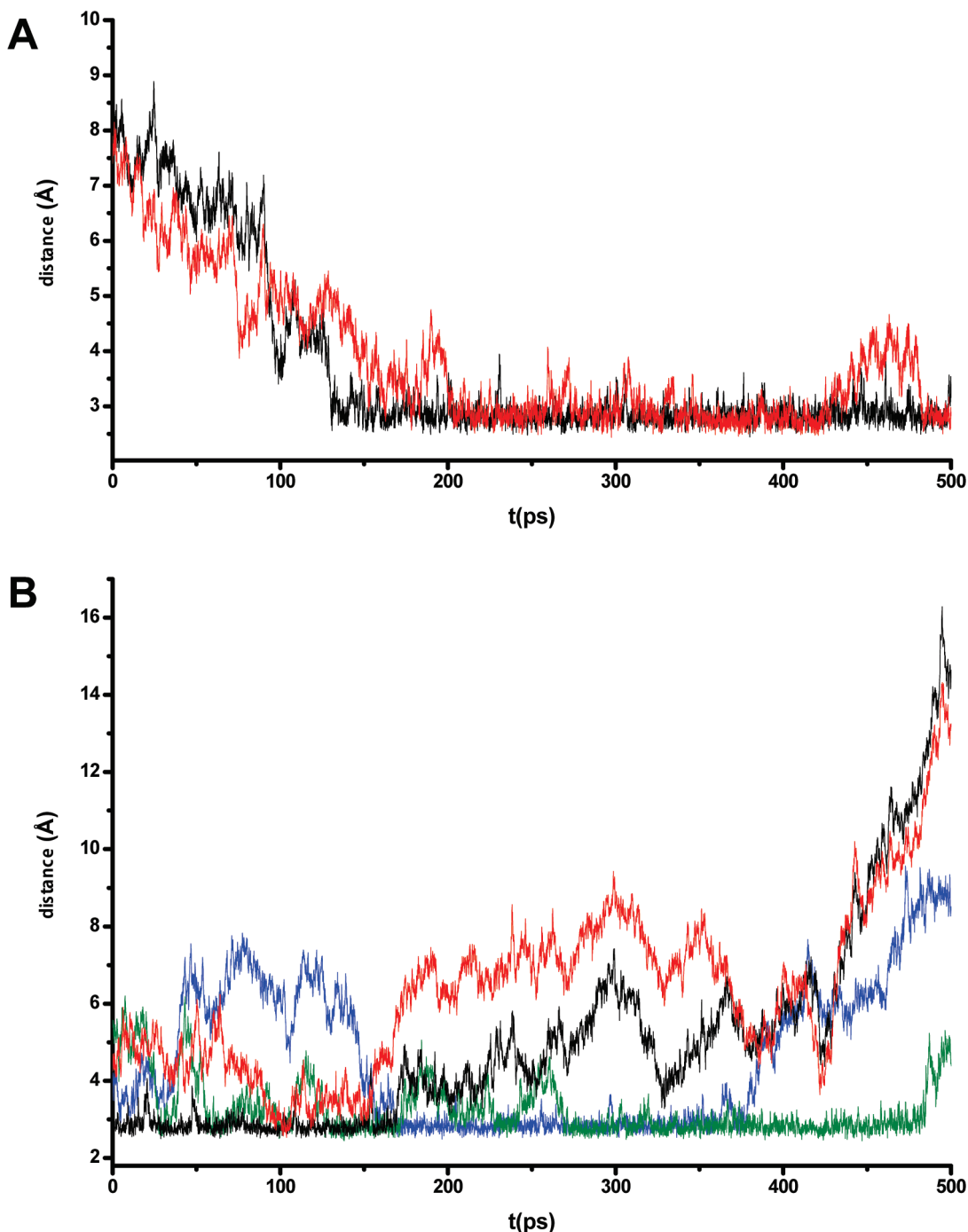


Figure 7. Distances of water molecules between the backbone of residue Ile10 and the sulfonamide oxygen O_2 of the inhibitor during simulations: (A) for the complex with **29**, where the distance between oxygen of water molecule and O_2 of compound **29** $D(\text{OWAT}-\text{O}_2\text{S})$ is represented in black and the distance between oxygen of water molecule and carbonylic oxygen from backbone of residue Ile10 $D(\text{OWAT}-\text{COIle10})$ is represented in red; (B) for the complex with **46**, where the distance between oxygen of water molecule WAT1 and O_2 of compound **46** $D(\text{OWAT1}-\text{O}_2\text{S})$ is represented in black, the distance between oxygen of water molecule WAT1 and carbonylic oxygen from backbone of residue Ile10 $D(\text{OWAT1}-\text{COIle10})$ is represented in red, the distance between oxygen of water molecule WAT2 and O_2 of the compound **46** $D(\text{OWAT2}-\text{O}_2\text{S})$ is represented in blue, and the distance between oxygen of water molecule WAT2 and carbonylic oxygen from backbone of residue Ile10 $D(\text{OWAT2}-\text{COIle10})$ is represented in green.

compounds during their simulations. O_2 of compounds **42** and **43** did not interact with any residue during their simulations (Figure 5B,C). However, the O_2 atoms of compounds **29** and **46** were able to interact with the backbone carbonyl group of residue Ile10 mediated by a water molecule from the solvent water box (Figure 5A,D); this corroborates our previous results for compound **29**.¹⁷ The importance of the structure and dynamics of water molecules in the active site of CDK2–inhibitor complexes has been

previously considered;³³ for this reason, we focus on water molecules involved in the interaction between the inhibitor and residue Ile10. Figure 7A shows the distances between the oxygen of a water molecule and the O_2 atom of compound **29** [$D(\text{OWAT}-\text{O}_2\text{S})$] and between the same water atom and the carbonylic oxygen from the backbone of residue Ile10 [$D(\text{OWAT}-\text{COIle10})$] during the simulation. In Figure 7A, when both distances were around 3 Å, a water bridge between the ligand and the binding site was established, as

Table 3. Average QM/MM Interaction Energies and Their Components (kcal/mol) for the CDK2 Inhibitors Studied

	compounds			
	29	42	43	46
interaction energy	-124.5 (± 8.2)	-122.9 (± 7.0)	-117.8 (± 5.7)	-138.3 (± 8.6)
electrostatic energy	-65.8 (± 9.0)	-62.1 (± 6.9)	-51.4 (± 5.9)	-77.6 (± 9.3)
vdW energy	-58.6 (± 3.0)	-60.8 (± 3.0)	-66.4 (± 2.6)	-60.7 (± 3.0)
log($10^3/\text{IC}_{50}$)	5.268	5.155	4.252	4.155

shown in Figure 5A. This behavior was shown in our simulation from 200 to 430 ps and then from 480 ps to the end of the simulation. The length of the water bridge in the CDK2–inhibitor system was rather long, implying a stable and strong connection. Two molecules of water denoted by WAT1 and WAT2 were able to form a similar water bridge in the complex between compound **46** and CDK2, during its 500-ps simulation. Figure 7B shows the distances between the oxygen atoms of water molecules WAT1 and WAT2 and the O₂ atom of compound **46** [$D(\text{OWAT1}-\text{O}_2\text{S})$ and $D(\text{OWAT2}-\text{O}_2\text{S})$, respectively] and between the same water atom and the carbonylic oxygen from the backbone of residue Ile10 [$D(\text{OWAT1}-\text{COIle10})$ and $D(\text{OWAT2}-\text{COIle10})$, respectively] during the simulation. When both distances were around 3 Å, a water bridge between the ligand and the binding site was established, as shown in Figure 5D. As can be seen in Figure 7B, molecule WAT1 interacted with O₂ of compound **46** until the beginning of the simulation, but the interaction with Ile10 was established only around 100 and 150 ps. At those moments, water bridges were formed, but they were not very stable. After the displacement of WAT1, the second water molecule WAT2 moved in and formed a similar bridge between 170 and 390 ps; after that, compound **46** changed its orientation, and the interaction was broken. We verified that compounds **42** and **43** did not establish water bridges with Ile10 throughout their entire simulation periods; moreover, compound **46** did not establish water bridges with Ile10 after 390 ps, when the ligand was reoriented. According to these results, we conclude that a water bridge between O₂ of the inhibitor and the backbone of Ile10 is formed when HBs between O₁ of the ligand and Lys89 and between nitrogen from the aminosulfonyl group and the carboxylic oxygens of Asp86 are formed.

Regarding the role of the water bridge between inhibitors and residue Ile10, as discussed previously, it can be hypothesized that Ile10 could act as an anchor, through the water molecule from the solvent environment, to stabilize the HB interactions with residues Asp86 and Lys89 for compound **29**. The unstable behavior of compound **46** regarding the above-mentioned interaction with Ile10 and water molecules reflects in some way the destabilizing effect caused by methoxy-group substitution at position 3 in the phenyl ring. In general, the low affinity (one order less than for compound **29**) of compound **46** can be attributed to the instabilities caused by phenyl-ring substitution in the HB interactions with residues at the ATP entrance channel within the CDK2 binding site.

In summary, HB interactions between inhibitors and the Lys89 residue of CDK2 have been previously reported.^{17,34} Lys89 is located at the entrance of the ATP binding site of CDK2; however, CDK4 has a threonine instead a lysine at this position. For this reason, it is implicated in defining CDK2/CDK4 inhibitor selectivity. Compound **29** (NU6102)

is highly potent and presents a good degree of selectivity for CDK2 against CDK4. As mentioned earlier, we found previously that sulfonamide oxygen atom O₁ of compound **29** accepts a HB from the NH₃⁺ side-chain group of Lys89;¹⁷ this has been corroborated in the current study. In addition, Heady et al. recently combined classical dynamic simulations with an ab initio computational approach for investigating the binding of several inhibitors of cyclin-dependent kinase CDK2.³⁵ Their simulations revealed the presence of intermittent HB interactions between the inhibitors NU6102 (compound **29** here), NU6027, and SU9516 and the Lys89 residue. Even though these interactions have not been identified in the crystallographic studies performed to date, they can be detected by considering molecular dynamic processes.

Water-bridge HB interactions between inhibitors and the Ile10 residue of CDK2 have also been previously reported. In the high-resolution crystals 2C6I and 2C6M, when aminosulfonyl-involved complexes were cocrystallized with CDK2, a water molecule was caught together by Ile10 and the inhibitor aminosulfonyl group, respectively.³⁴ We found that the water bridge HB is formed only for compounds containing an aminosulfonyl group. When the aminosulfonyl group was replaced by (methylamino)sulfonyl or (dimethylamino)sulfonyl groups, the water molecule could no longer be detected. According to these observations, it seems that the binding of the studied analogues could be improved by replacing the water molecule between Ile10 and the aminosulfonyl group with a H-bond-donor-substituted aminosulfonyl group capable of establishing a stronger interaction with the backbone of Ile10.

To rationalize the interactions described in the sections above, we performed an energy analysis within the framework of the QM/MM approach, and we examined its relationship with biological activity for the compounds studied. Energy data terms were averaged during the production run, and the standard deviations are provided as numbers in parentheses accompanying the averaged values. As shown in Table 3, the interaction energy can be split in two terms: the electrostatic and van der Waals (vdW) energy terms. The biological activity is also provided as the logarithm of ($10^3/\text{IC}_{50}$). The potency of each ligand is obviously related to its binding free energy, assuming that, within a family of compounds, solvation/desolvation energies, enzyme deformation energy, and entropic changes are proportional to the magnitude of the interactions established between the inhibitor and the protein.

Overall, the interaction energy can explain fairly well the affinities for three of the four compounds studied. The interaction energy for compound **29** has a value of -124.5 kcal/mol, and the electrostatic component outweighs the vdW, as expected according to the network of HB interactions formed by this compound with residues Ile10, Asp86, and Lys89. The interaction energies for compounds **42** and

43 take values of -122.9 and -117.8 kcal/mol, respectively. This trend is in agreement with the experimental activities reported for these compounds. It is interesting to see how the electrostatic component diminishes (in absolute value) for these compounds according to the replacement of H atoms by methyl groups in the sulfonamide moiety and the consequent loss of some HB interactions. The change in this energy component for compound **43**, with respect to compound **29**, is about -14.4 kcal/mol, and it reflects the magnitude of the HB interaction with the side chain of residue Asp86. On the other hand, the vdW component increases (in absolute value) when methyl groups are added to the sulfonamide moiety. For this case, the vdW component outweighs the electrostatic component in compound **43** and confirms the loss of the HBs network for this ligand and the impact in its potency.

Unfortunately, our approach could not explain the energetic behavior for compound **46**. In our previous work (ref 19), the interaction energy calculation also failed for compound **46** when the hybrid ONIOM method was used. The high interaction energy calculated for this compound can be rationalized in terms of the many HBs that it can establish with residues at the CDK2 active site, as revealed in the electrostatic component value. However, this does not reflect the low stability of the HB interactions as analyzed in the simulations described before. A high level of theory in the quantum mechanical region would be needed to obtain more accurate results for the interaction energy and its component for this set of compounds.

In general, the method allowed us to partially explain the effects of the substitution pattern in the sulfonamide moiety, and it captured the changes in the electrostatic and van der Waals energy components as the HB network changed.

CONCLUSIONS

Quantitative structure–activity relationships and QM/MM hybrid studies were conducted to establish relevant features describing the CDK2 inhibitory activity of 9*H*-purine derivatives. First, a predictive CoMFA model was built. A reliable model was derived by using steric and electrostatic fields. Thus, prediction of CDK2 activities with sufficient accuracy should be possible. Moreover, an interpretation of the CoMFA fields makes it possible to draw conclusions concerning the most appropriate features for the analogues. The reported models have the potential to discover new potent inhibitors and provide useful molecular information about ligand specificity for interacting with the CDK2 binding pocket.

Second, the dynamics of the interactions of selected N2 substituents in the purine scaffold with residues in the CDK2 active site was analyzed. For this purpose, QM/MM simulations of compounds containing 4-(aminosulfonyl)phenyl, 4-[(methylamino)sulfonyl]phenyl, 4-[(dimethylamino)sulfonyl]phenyl, and [3-methoxy-4-(aminosulfonyl)]phenyl groups were carried out. We found that the 4-(aminosulfonyl)phenyl group forms HB interactions between O₁ of the ligand and Lys89 and between nitrogen from the aminosulfonyl group and the carboxylic oxygens of Asp86; in addition, it forms a water-bridge-mediated HB interaction between O₂ of the inhibitor and backbone of Ile10. These interactions were stable for the compound containing a 4-(aminosulfonyl)phe-

nyl group, but not very stable for the compound containing a [3-methoxy-4-(aminosulfonyl)]phenyl group. It can be stated that, despite the extended HB network formed by compound **46** within the CDK2 binding site, these interactions are not stable enough to achieve an efficient binding to the enzyme. Furthermore, the above-mentioned interactions were not established for compounds containing 4-[(methylamino)sulfonyl]phenyl and 4-[(dimethylamino)sulfonyl]phenyl groups.

The important role of residues Lys89 and Asp86 (specifically the side chain) in the affinity of compound **29** has been confirmed, and the role of residue Ile10 (and a water molecule) as an anchor to improve the interactions with the mentioned residues has been proposed.

The QM/MM method allowed us to rationalize the interactions of compounds within the CDK2 binding site in terms of the interaction energy and partially permitted us to explain the relative importance of the electrostatic and van der Waals energy terms in these protein–ligand interactions.

ACKNOWLEDGMENT

J.A.-M. acknowledges PBCT (Programa Bicentenario de Ciencia y Tecnología) for the postdoctoral fellowship PSD-086. The authors also acknowledge “Programa Bicentenario de Ciencia y Tecnología”, ACT/24.

REFERENCES AND NOTES

- Harper, J. W.; Adams, P. D. Cyclin-Dependent Kinases. *Chem. Rev.* **2001**, *101*, 2511–2526.
- Vermeulen, K.; Berneman, Z. N.; Van Bockstaele, D. R. Cell cycle and apoptosis. *Cell Proliferation* **2003**, *36*, 165–175.
- Morgan, D. O. Principles of CDK regulation. *Nature* **1995**, *374*, 131–134.
- Malumbres, M.; Barbacid, M. Milestones in cell division: To cycle or not to cycle: A critical decision in cancer. *Nat. Rev. Cancer* **2001**, *1*, 222–231.
- Malumbres, M.; Pevalero, P.; Barbacid, M.; Bischoff, J. R. CDK inhibitors in cancer therapy: What is next? *Trends Pharmacol. Sci.* **2008**, *29*, 16–21.
- Senderowicz, A.; Headlee, D.; Stinson, S.; Lush, R.; Kalil, N.; Villalba, L.; Hill, K.; Steinberg, S.; Figg, W.; Tompkins, A.; Arbuck, S.; Sausville, E. Phase I trial of continuous infusion flavopiridol, a novel cyclin-dependent kinase inhibitor, in patients with refractory neoplasms. *J. Clin. Oncol.* **1998**, *16*, 2986–2999.
- Fuse, E.; Kuwabara, T.; Sparreboom, A.; Sausville, E. A.; Figg, W. D. Review of UCN-01 Development: A Lesson in the Importance of Clinical Pharmacology. *J. Clin. Pharmacol.* **2005**, *45*, 394–403.
- Meijer, L.; Borgne, A.; Mulner, O.; Chong, J. P. J.; Blow, J. J.; Inagaki, N.; Inagaki, M.; Delcros, J.; Moulinoux, J. P. Biochemical and Cellular Effects of Roscovitine, a Potent and Selective Inhibitor of the Cyclin-Dependent Kinases cdc2, cdk2 and cdk5. *Eur. J. Biochem.* **1997**, *243*, 527–536.
- Misra, R. N.; Xiao, H.; Kim, K. S.; Lu, S.; Han, W.; Barbosa, S. A.; Hunt, J. T.; Rawlins, D. B.; Shan, W.; Ahmed, S. Z.; Qian, L.; Chen, B.; Zhao, R.; Bednarz, M. S.; Kellar, K. A.; Mulheron, J. G.; Batorsky, R.; Roongta, U.; Kamath, A.; Marathe, P.; Ranadive, S. A.; Sack, J. S.; Tokarski, J. S.; Pavletich, N. P.; Lee, F. Y. F.; Webster, K. R.; Kimball, S. D. N-(Cycloalkylamino)acyl-2-aminothiazole Inhibitors of Cyclin-Dependent Kinase 2. N-[5-[[5-(1,1-Dimethylethyl)-2-oxoazolyl]methyl]thio]-2-thiazolyl]-4-piperidinecarboxamide (BMS-387032), a Highly Efficacious and Selective Antitumor Agent. *J. Med. Chem.* **2004**, *47*, 1719–1728.
- McInnes, C. Progress in the evaluation of CDK inhibitors as anti-tumor agents. *Drug Discov. Today* **2008**, *13*, 875–881.
- Kelland, L. R. *Inhibitors of Cyclin-Dependent Kinases as Anti-Tumor Agents*; CRC Press: Boca Raton, FL, 2007; pp 371–388.
- Fernandez, M.; Tundidor-Camba, A.; Caballero, J. Modeling of Cyclin-Dependent Kinase Inhibition by 1H-Pyrazolo[3,4-d]Pyrimidine Derivatives Using Artificial Neural Network Ensembles. *J. Chem. Inf. Model.* **2005**, *45*, 1884–1895.
- González, M.; Caballero, J.; Helguera, A.; Garriga, M.; González, G.; Fernández, M. 2D Autocorrelation Modelling of the Inhibitory Activity

- of Cytokinin-Derived Cyclin-Dependent Kinase Inhibitors. *Bull. Math. Biol.* **2006**, *68*, 735–751.
- (14) Caballero, J.; Fernández, M.; González-Nilo, F. D. Structural requirements of pyrido[2,3-d]pyrimidin-7-one as CDK4/D inhibitors: 2D autocorrelation, CoMFA and CoMSIA analyses. *Bioorg. Med. Chem.* **2008**, *16*, 6103–6115.
 - (15) Cramer, R. D.; Patterson, D. E.; Bunce, J. D. Comparative molecular field analysis (CoMFA). 1. Effect of shape on binding of steroids to carrier proteins. *J. Am. Chem. Soc.* **1988**, *110*, 5959–5967.
 - (16) Klebe, G.; Abraham, U.; Mietzner, T. Molecular Similarity Indices in a Comparative Analysis (CoMSIA) of Drug Molecules to Correlate and Predict Their Biological Activity. *J. Med. Chem.* **1994**, *37*, 4130–4146.
 - (17) Alzate-Morales, J. H.; Contreras, R.; Soriano, A.; Tuñon, I.; Silla, E. A Computational Study of the Protein–Ligand Interactions in CDK2 Inhibitors: Using Quantum Mechanics/Molecular Mechanics Interaction Energy as a Predictor of the Biological Activity. *Biophys. J.* **2007**, *92*, 430–439.
 - (18) Alzate-Morales, J. H.; Tiznado, W.; Santos, J. C.; Cardenas, C.; Contreras, R. Theoretical Study on CDK2 Inhibitors Using a Global Softness Obtained from the Density of States. *J. Phys. Chem. B* **2007**, *111*, 3293–3297.
 - (19) Alzate-Morales, J. H.; Caballero, J.; Vergara-Jaque, A.; González-Nilo, F. D. Insights into the structural basis of N2 and O6 substituted guanine derivatives as cyclin-dependent kinase 2 (CDK2) inhibitors: Prediction of the binding modes and potency of the inhibitors by docking and ONIOM calculations. *J. Chem. Inf. Model.* **2009**, *49*, 886–899.
 - (20) Hardcastle, I. R.; Arris, C. E.; Bentley, J.; Boyle, F. T.; Chen, Y.; Curtin, N. J.; Endicott, J. A.; Gibson, A. E.; Golding, B. T.; Griffin, R. J.; Jewsbury, P.; Menyerol, J.; Mesguiche, V.; Newell, D. R.; Noble, M. E. M.; Pratt, D. J.; Wang, L. Z.; Whitfield, H. J. N2-Substituted O6-Cyclohexylmethylguanine Derivatives: Potent Inhibitors of Cyclin-Dependent Kinases 1 and 2. *J. Med. Chem.* **2004**, *47*, 3710–3722.
 - (21) Gibson, A. E.; Arris, C. E.; Bentley, J.; Boyle, F. T.; Curtin, N. J.; Davies, T. G.; Endicott, J. A.; Golding, B. T.; Grant, S.; Griffin, R. J.; Jewsbury, P.; Johnson, L. N.; Mesguiche, V.; Newell, D. R.; Noble, M. E. M.; Tucker, J. A.; Whitfield, H. J. Probing the ATP Ribose-Binding Domain of Cyclin-Dependent Kinases 1 and 2 with O6-Substituted Guanine Derivatives. *J. Med. Chem.* **2002**, *45*, 3381–3393.
 - (22) Griffin, R. J.; Henderson, A.; Curtin, N. J.; Echalier, A.; Endicott, J. A.; Hardcastle, I. R.; Newell, D. R.; Noble, M. E. M.; Wang, L. Z.; Golding, B. T. Searching for Cyclin-Dependent Kinase Inhibitors Using a New Variant of the Cope Elimination. *J. Am. Chem. Soc.* **2006**, *128*, 6012–6013.
 - (23) Arris, C. E.; Boyle, F. T.; Calvert, A. H.; Curtin, N. J.; Endicott, J. A.; Garman, E. F.; Gibson, A. E.; Golding, B. T.; Grant, S.; Griffin, R. J.; Jewsbury, P.; Johnson, L. N.; Lawrie, A. M.; Newell, D. R.; Noble, M. E. M.; Sausville, E. A.; Schultz, R.; Yu, W. Identification of Novel Purine and Pyrimidine Cyclin-Dependent Kinase Inhibitors with Distinct Molecular Interactions and Tumor Cell Growth Inhibition Profiles. *J. Med. Chem.* **2000**, *43*, 2797–2804.
 - (24) SYBYL, version 7.3; Tripos Inc.: St. Louis, MO, 2006.
 - (25) Bush, B. L.; Nachbar, R. B. Sample-distance partial least squares: PLS optimized for many variables, with application to CoMFA. *J. Comput.-Aided Mol. Des.* **1993**, *7*, 587–619.
 - (26) Field, M. J.; Albe, M.; Bret, C.; Proust-De Martin, F.; Thomas, A. The dynamo library for molecular simulations using hybrid quantum mechanical and molecular mechanical potentials. *J. Comput. Chem.* **2000**, *21*, 1088–1100.
 - (27) Dewar, M. J. S.; Zoebisch, E. G.; Healy, E. F.; Stewart, J. J. P. Development and use of quantum mechanical molecular models. 76. AM1: A new general purpose quantum mechanical molecular model. *J. Am. Chem. Soc.* **1985**, *107*, 3902–3909.
 - (28) Jorgensen, W. L.; Maxwell, D. S.; Tirado-Rives, J. Development and Testing of the OPLS All-Atom Force Field on Conformational Energetics and Properties of Organic Liquids. *J. Am. Chem. Soc.* **1996**, *118*, 11225–11236.
 - (29) Jorgensen, W. L.; Chandrasekhar, J.; Madura, J. D.; Impey, R. W.; Klein, M. L. Comparison of simple potential functions for simulating liquid water. *J. Chem. Phys.* **1983**, *79*, 926–935.
 - (30) Steinbach, P. J.; Brooks, B. R. New spherical-cutoff methods for long-range forces in macromolecular simulation. *J. Comput. Chem.* **1994**, *15*, 667–683.
 - (31) Gao, J.; Truhlar, D. G. Quantum Mechanical Methods for Enzyme Kinetics. *Annu. Rev. Phys. Chem.* **2002**, *53*, 467–505.
 - (32) Caballero, J.; Fernández, M.; González-Nilo, F. D. A CoMSIA study on the adenosine kinase inhibition of pyrrolo[2,3-d]pyrimidine nucleoside analogues. *Bioorg. Med. Chem.* **2008**, *16*, 5103–5108.
 - (33) Zhang, B.; Tan, V. B. C.; Lim, K. M.; Tay, T. E. Significance of Water Molecules in the Inhibition of Cyclin-Dependent Kinase 2 and 5 Complexes. *J. Chem. Inf. Model.* **2007**, *47*, 1877–1885.
 - (34) Richardson, C. M.; Williamson, D. S.; Parratt, M. J.; Borgognoni, J.; Cansfield, A. D.; Dokurno, P.; Francis, G. L.; Howes, R.; Moore, J. D.; Murray, J. B.; Robertson, A.; Surgenor, A. E.; Torrance, C. J. Triazolo[1,5-a]pyrimidines as novel CDK2 inhibitors: Protein structure-guided design and SAR. *Bioorg. Med. Chem. Lett.* **2006**, *16*, 1353–1357.
 - (35) Heady, L.; Fernandez-Serra, M.; Mancera, R. L.; Joyce, S.; Venkitaraman, A. R.; Artacho, E.; Skylaris, C. K.; Ciacchi, L. C.; Payne, M. C. Novel Structural Features of CDK Inhibition Revealed by an ab Initio Computational Method Combined with Dynamic Simulations. *J. Med. Chem.* **2006**, *49*, 5141–5153.

CI900302Z